QUARTERLY OF APPLIED MATHEMATICS

VISCOUS FLOW ALONG A CORNER:

NUMERICAL SOLUTION OF THE CORNER LAYER EQUATIONS*

BY

STANLEY G. RUBIN AND BERNARD GROSSMAN

Polytechnic Institute of Brooklyn Graduate Center, Farmingdale, New York

Abstract. Solutions for the viscous incompressible flow along a right-angle corner have been found by a method of successive iteration. The algebraic nature of the asymptotic flow field has been utilized to provide boundary conditions for the numerical analysis. One arbitrary constant appearing in the asymptotic series has been determined by the elimination of interior mass sources that appear as a result of any inaccuracy in the value of this constant, allowing additional mass to cross the outer boundary. The numerical solution shows a swirling flow in the corner but a closed vortical pattern is not established.

1. Introduction. The viscous flow along a right-angle corner has been reconsidered by Rubin [1]. In his analysis the flow was partitioned into the three regions depicted in Fig. 1, and solutions for the boundary layer and potential flow were obtained by the method of matched asymptotic expansions. The asymptotic boundary values, as $\zeta \to \infty$, required for the corner layer solution were determined by the proper matching of the flows in the three regions.

When numerical solution of the elliptic corner layer equations was initiated, it became clear that conjectured exponential decay of the velocities and streamwise vorticity from the corner layer into the boundary layer was not realized. As it was not practical in the numerical analysis to apply the asymptotic conditions, strictly valid only for the coordinate $\zeta \to \infty$, for values of ζ excess of ten or twenty, additional consideration of the asymptotic behavior was required in order to describe the proper algebraic decay. A detailed asymptotic analysis is presented by Pal and Rubin [2], where the existence of consistent asymptotic series exhibiting the necessary algebraic behavior is formally demonstrated. Of particular significance for the numerical analysis is the appearance of arbitrary constants and logarithmic terms in these expansions.

The analysis contained herein is concerned with a numerical solution of the corner layer equations, taking proper account of the asymptotic formulas discussed in [2] The system of equations for the corner layer region is transformed into four Poisson-
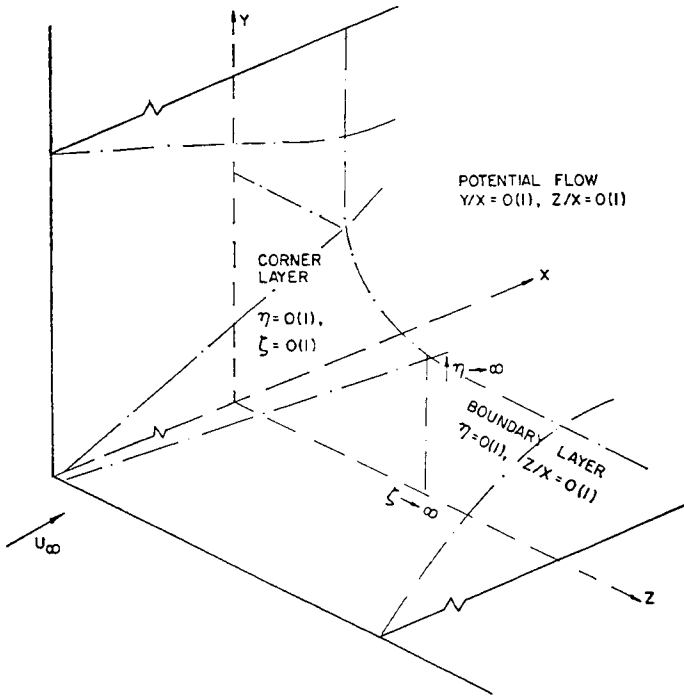
FIG. 1.   Corner flow geometry.

like equations for the streamwise velocity, suitably modified cross-plane velocities, and a modified streamwise vorticity. This system includes only differentiated forms of the mass continuity equation and vorticity definition and is similar to that described previously by Pearson [3]. For the asymptotic boundary values the series solution obtained in [2] is required. In view of the nature of the asymptotic expansion discussed in [2], sufficient accuracy for the numerical analysis is obtained by retaining only terms up to $O(\zeta^2[\eta^2 + \zeta^2]^{-2})$. This leads to the inclusion of a single unknown constant χ; moreover, logarithmic effects are avoided as they first appear in terms of $O(\zeta^{-5})$.

Solutions are obtained numerically by the Gauss-Seidel method of successive iteration with the asymptotic values applied at $\zeta = Z \leq 15$. From the results of [2] it is apparent that any inaccuracy $[\chi]$ in the constant χ at the asymptotic boundary will result in an increased error of $O([\chi]Z^{-1})$ in the asymptotic conditions, above the usual error associated with the termination of the series. This inaccuracy is reflected in the mass flux crossing the boundary $\zeta = Z$. Using an iterative procedure, an optimum value for χ is obtained by minimizing the errors associated with the undifferentiated mass continuity equation, i.e., eliminating interior mass sources. Systematic consideration of the effects of Z, χ, or grid spacing was facilitated by the use of a CDC 6600 computer.

2. Mathematical formulation.   The similarity equations valid downstream of the leading edge $x = 0$ and governing the viscous incompressible corner layer flow are obtained as the leading terms in an expansion of the Navier-Stokes equations for $R = (2U_0x/\nu) \gg 1$ (Rubin [1]). With

$$u(x, y, z) = U_0u(\eta, \zeta), \qquad v(x, y, z) = U_0R^{-1/2}v(\eta, \zeta),$$

$$w(x, y, z) = U_0R^{-1/2}w(\eta, \zeta), \qquad \eta = y(U_0/2\nu x)^{1/2}, \qquad \zeta = z(U_0/2\nu x)^{1/2},$$

the corner layer equations as reformulated in [2] become

$$u_{\eta\eta} + u_{\zeta\zeta} + \varphi u_{\eta} + \psi u_{\zeta} = 0, \tag{2.1a}$$

$$\theta_{\eta\eta} + \theta_{\zeta\zeta} + \varphi\theta_{\eta} + \psi\theta_{\zeta} + 2u(\theta - \zeta u_{\eta} + \eta u_{\zeta}) = 0, \tag{2.1b}$$

$$\varphi_{\eta} + \psi_{\zeta} - 2u = 0, \tag{2.2a}$$

$$\psi_{\eta} - \varphi_{\zeta} - \theta = 0. \tag{2.2b}$$

The cross-velocities $v(\eta, \zeta)$ and $w(\eta, \zeta)$ in the η, ζ direction respectively are related to φ, ψ, u by

$$v = \eta u - \varphi \qquad w = \zeta u - \psi \tag{2.3a}$$

and the streamwise vorticity $\Omega = w_{\eta} - v_{\zeta}$ is given by

$$\Omega = \zeta u_{\eta} - \eta u_{\zeta} - \theta. \tag{2.3b}$$

Alternate forms for the continuity Eq. (2.2a) and vorticity relation (2.2b) are obtained by cross-differentiating so that

$$\varphi_{\eta\eta} + \varphi_{\zeta\zeta} + \theta_{\zeta} - 2u_{\eta} = 0, \tag{2.4a}$$

$$\psi_{\eta\eta} + \psi_{\zeta\zeta} - \theta_{\eta} - 2u_{\zeta} = 0. \tag{2.4b}$$

Eqs. (2.1) and (2.4) constitute a set of four nonlinear elliptic Poisson-like equations for which relaxation methods are generally well suited. The appropriate boundary conditions are, at the surface $\eta = 0$,

$$\varphi = \psi = u = 0, \tag{2.5a}$$

$$\theta = \psi_{\eta}, \tag{2.5b}$$

while from symmetry, across $\eta = \zeta$,

$$u_{\eta} = u_{\zeta}, \qquad \varphi = \psi, \qquad \varphi_{\zeta} = \psi_{\eta}, \tag{2.5c}$$

$$\theta = 0. \tag{2.5d}$$

From the analysis of [2] the asymptotic behavior as $\zeta \to \infty$ is the following:

(i) $\min(\eta, \zeta) \to \infty$: Corner Layer $\to$ Potential Flow.

$$u \sim 1 + o(\eta^{-N}), \qquad \theta \sim o(\eta^{-M}), \quad \text{for arbitrary } N, M. \tag{2.6a}$$

$$e^{i\pi/4}(\varphi - i\psi) \sim (\eta - i\zeta)e^{i\pi/4} - (2)^{1/2}\beta + 4\chi\tau^{-1} + (2)^{1/2}\beta\chi\tau^{-2} + \sum_{n=3}^{\infty}\gamma_n(\log\tau)\tau^{-n}. \tag{2.6b}$$

where $\tau = (\eta + i\zeta)e^{-i\pi/4}$; γ_n is real with a log ζ term first appearing in γ_5. χ is a real constant yet to be determined and

$$\beta = \lim_{\eta\to\infty}(\eta f'(\eta) - f(\eta)) = 1.21678;$$

$f(\eta)$ is the familiar Blasius flat plate solution (Rosenhead [4]).

(ii) $\zeta \to \infty$, $\eta/\zeta \to 0$: Corner Layer $\to$ Boundary Layer.

$$u \sim f'(\eta) + \chi\eta f''(\eta)\zeta^{-2} + O(\zeta^{-3}), \tag{2.7a}$$

$$\theta \sim \zeta f''(\eta) - \beta g'(\eta) + \chi f''(\eta)[5 - \eta f(\eta)]\zeta^{-1} + \chi\beta h'(\eta)\zeta^{-2} + O(\zeta^{-3}), \tag{2.7b}$$

$$\phi \sim f(\eta) + \chi[3\eta f'(\eta) + f(\eta)]\zeta^{-2} + O(\zeta^{-3}), \tag{2.7c}$$

$$\psi \sim \zeta f'(\eta) - \beta g(\eta) + \chi[\eta f''(\eta) + 4f'(\eta)]\zeta^{-1} + \beta \chi h(\eta)\zeta^{-2} + O(\zeta^{-3}), \tag{2.7d}$$

where

$$g(\eta) = f''(\eta) \int_0^\eta [(\tau - \beta)/f''(\tau)] \, d\tau,$$

and $h(\eta)$ is determined numerically (see Appendix I). For the numerical computation only terms up to $O(\zeta^{-2})$ or $O(\tau^{-2})$ will be retained. Therefore, the asymptotic boundary conditions as obtained from a composite expansion of (2.6) and (2.7) become:

$$u = f'(\eta) + \chi\eta f''(\eta)\zeta^{-2}, \tag{2.8a}$$

$$\theta = \zeta f''(\eta) - \beta g'(\eta) + \chi\{f''(\eta)[5 - \eta f(\eta)]\zeta^{-1} + \beta h'(\eta)\zeta^{-2}\}, \tag{2.8b}$$

$$\varphi = f(\eta) + \chi\{[3\eta f'(\eta) + f(\eta) - 4\eta + \beta]\zeta^{-2} + 4\eta(\eta^2 + \zeta^2)^{-1}$$
$$+ \beta(\eta^2 + 2\eta\zeta - \zeta^2)(\eta^2 + \zeta^2)^{-2}\}, \tag{2.8c}$$

$$\psi = \zeta f'(\eta) - \beta g(\eta) + \chi\{[\eta f''(\eta) + 4f'(\eta) - 4]\zeta^{-1}$$
$$+ \beta[h(\eta) - 1]\zeta^{-2} + 4\zeta(\eta^2 + \zeta^2)^{-1} - \beta(\eta^2 - 2\eta\zeta - \zeta^2)(\eta^2 + \zeta^2)^{-2}\}. \tag{2.8d}$$

The symmetry conditions (2.5c) and (2.5d) are automatically satisfied by the above relations when $\zeta \to \infty$, $\eta = \zeta$ (cf. [2]).

The error associated with the truncated series (2.8) can be expected to be of $O(\zeta^{-3})$; however, due to the typically divergent nature of such asymptotic expansions it was found that the magnitude of the first neglected term in any of the formulas (2.8) or equations (2.1) could be represented as $E(\eta)\zeta^{-3}$, and that $|E(\eta)| \leq 35$, except for (2.8c) where local values of $E(\eta) \approx 70$ occur (see Appendix I).[1] For $\zeta = X = 15$, the series truncation error should then be at most 0.03; therefore, the final numerical solutions were determined with $Z = 15$. The effect of smaller Z values is discussed in Sec. 3.

With the boundary conditions (2.5) and (2.8), and the system of equations (2.1) and (2.4), the problem is completely specified. It is significant to note that although the final system includes the differentiated equations (2.4), the prescribed boundary conditions guarantee that Eqs. (2.2) are also satisfied. For it would appear that if the right-hand sides of (2.2a) and (2.2b) were instead of zero, $2C(\eta, \zeta)$ and $V(\eta, \zeta)$ respectively, Eqs. (2.4) would still be satisfied for any harmonic functions C and V; i.e.,

$$C_{\eta\eta} + C_{\zeta\zeta} = 0, \qquad V_{\eta\eta} + V_{\zeta\zeta} = 0. \tag{2.9}$$

Since we are seeking solutions for which C and V are to vanish everywhere, the boundary conditions (2.5) and (2.8) must insure that C and V are zero on at least part of the corner boundary with the normal gradients, e.g., C_η on $\eta = 0$, zero elsewhere on the boundary. From (2.5a), (2.5b) we obtain $V = 0$ on $\eta = 0$ and with (2.4a), $C_\eta = 0$ on $\eta = 0$. The symmetry conditions (2.5c) and (2.5d) insure that along the diagonal $\eta = \zeta$, both V and the normal gradient of C vanish; i.e., $V = 0$ and $C_\eta - C_\zeta = 0$. Finally, the asymptotic conditions (2.8) are such that $C = 0$ and $V = 0$, as they result from an asymptotic expansion of Eqs. (2.1) (cf. [2]). Of particular significance in this regard is the constant

---

[1] In view of the nature of the series (2.7), for $Z \leq 15$ the accuracy of the calculation would not be appreciably increased by including an additional term in (2.8).

χ. For any inaccuracy in this value leads to an error in the flow properties at the boundary of $O([\chi]Z^{-1})$, in addition to the error associated with the termination of series (2.8). Therefore, the finite difference representations for C and V at $\zeta = Z$ will also be in error. Eqs. (2.2) will be satisfied to the accuracy of the finite difference scheme and the maximum accuracy allowed by the series (2.8) only when the error in χ is a minimum. Therefore, the boundary conditions (2.5) and (2.8) insure that (2.2) will be satisfied. The proper choice of the constant χ is achieved when the functions $C(\eta, \zeta)$ and $V(\eta, \zeta)$ attain their minimum absolute values.

3. Numerical analysis. The governing equations are written in finite difference form with the use of five-point central difference formulas (see Appendix II). The following equations result:

$$8u_0 = u_1(2 + \varphi_0 t) + u_2(2 + \psi_0 t) + u_3(2 - \varphi_0 t) + u_4(2 - \psi_0 t), \qquad (3.1a)$$

$$4\theta_0(2 + u_0 t^2) = \theta_1(2 + \varphi_0 t) + \theta_2(2 + \psi_0 t) + \theta_3(2 - \varphi_0 t)$$
$$+ \theta_4(2 - \psi_0 t) - 2u_0 t[\zeta_0(u_1 - u_3) - \eta_0(u_2 - u_4)] \qquad (3.1b)$$

$$4\varphi_0 = \varphi_1 + \varphi_2 + \varphi_3 + \varphi_4 - (u_1 - u_3)t + (\theta_2 - \theta_4)(t/2), \qquad (3.1c)$$

$$4\psi_0 = \psi_1 + \psi_2 + \psi_3 + \psi_4 - (u_2 - u_4)t - (\theta_1 - \theta_3)(t/2), \qquad (3.1d)$$

where the grid points are defined in Fig. 2 and t is the uniform grid spacing. The boundary conditions are prescribed by (2.5) and (2.8), with the asymptotic values (2.8) applied at $\zeta = Z$. The vorticity at the surface $\eta = 0$ is specified by a three-point end difference formula having an error equivalent to that of (3.1):

$$\theta_w = (2t)^{-1}(4\psi_i - \psi_{ii}). \qquad (3.2)$$

From the symmetry conditions (2.5c), (2.5d) across $\eta = \zeta$,

$$u_a = u_a', \qquad \varphi_a = \psi_a', \qquad \psi_a = \varphi_a', \qquad \theta_a = -\theta_{a'}. \qquad (3.3)$$

Solutions of (3.1) are obtained by the Gauss-Seidel method of successive iteration (Smith [5]). Initial values for φ, ψ, u, θ are selected such that $C(\eta, \zeta)$ and $V(\eta, \zeta)$ are zero throughout. The prescribed initial values are

$$u(\eta, \zeta) = f'(\eta)f'(\zeta) + [(\alpha - \beta)/\beta]\eta\zeta f''(\eta)f''(\zeta),$$

$$v(\eta, \zeta) = [\eta f'(\eta) - f(\eta)]g(\zeta) + \zeta f''(\zeta)\left[f(\eta) - \int_0^\eta g(\eta)\, d\eta\right]$$

$$+ [(\alpha - \beta)/\beta]\zeta f''(\zeta)[\eta^2 f''(\eta) - \eta f'(\eta) + f(\eta)], \qquad (3.4)$$

$$w(\eta, \zeta) = v(\zeta, \eta),$$

$$\theta(\eta, \zeta) = \zeta u_\eta - \eta u_\zeta + v_\zeta - w_\eta,$$

where

$$\alpha = \lim_{\eta\to\infty}\left(\int_0^\eta g(\eta)\, d\eta - \eta\right) = 6.11456.$$

These initial conditions exhibit exponential decay for $\zeta \to \infty$; however, in this iterative method the algebraic nature of the asymptotic flow field appears very rapidly, after about 50 iterations.

The iteration procedure begins on the diagonal at the lower left-hand corner of the triangular domain of Fig. 2, one grid point above the surface $\eta = 0$. The point being considered is denoted by subscript zero in Eqs. (3.1). Utilizing the initial values for points 1, 2, 3 and φ_0, ψ_0, θ_0, a new value of u is obtained from (3.1a). This result immediately replaces the initial value of u_0. θ_0 is determined from (3.1b), φ_0 from (3.1c) and ψ_0 from (3.1d); the new values are used as they become available. The calculation then proceeds point by point to the right until all new values have been determined for this row. After the point $\zeta = Z - t$, the computation returns to the diagonal, incrementing η by t. The procedure continues until all grid points have been treated; this results in one complete iteration. The number of iterations required prior to convergence depends upon the grid spacing t and the boundary limit Z. If the solution is said to be converged when changes in successive iterations are less than one percent everywhere, then Table 1 lists the required number of iterations and respective calculation times on the CDC 6600 computer.

The error associated with any of the converged solutions is a function of the error inherent in the finite-difference approximation, the truncation error, at the boundary, in series (2.8), and any inaccuracy associated with the constant χ. Neglecting the effect of the latter for the moment, it is estimated that the first two are $O(t^2)$ and $O(E(\eta)Z^{-3})$ respectively. Therefore, with $t = 0.2$ and $Z = 15$, inaccuracies due to grid size are perhaps somewhat larger than those associated with the choice of the asymptotic boundary. As discussed previously, at the boundary the series truncation error with $Z = 15$ is less than 0.03. The finite-difference error can be further reduced by decreasing t; however, this is extremely time-consuming and leads to computer storage difficulties. On the other hand, for the system (3.1) and boundary conditions (2.5) describing the rectangular corner layer region, this error should be $O(t^2)$. Therefore, if σ_1 and σ_2 are
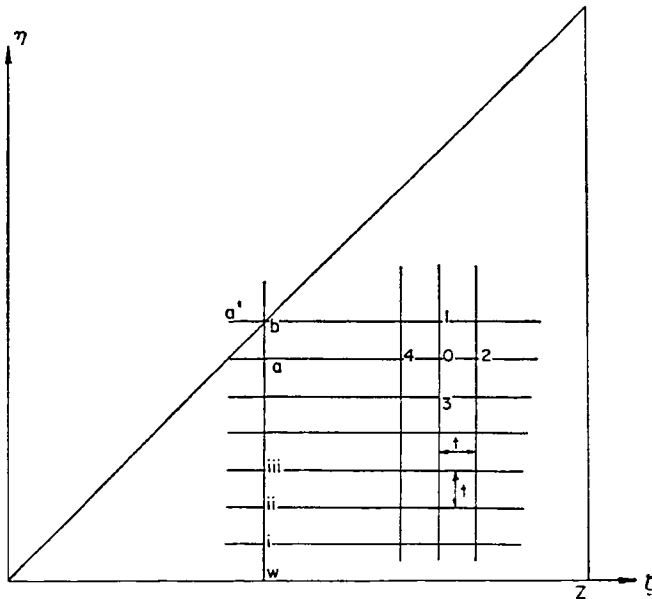

FIG. 2.   Finite difference grid.

TABLE 1

	Starting Conditions	t	Z	No. of Iterations	Calculation Time
(i)	Initial Conditions (3.4)	0.6	8.8	3000	1.0 min
(ii)	Initial Conditions (3.4)	0.4	10	4200	2.5 miu
(iii)	Converged Solution of (ii) Simple Average for Intermediate Values	0.2	10	2500	5.2 min
(iv)	Converged Solution of (iii) with Conditions (2.8) from $Z = 10$ to $Z = 15$	0.2	15	2000	9.5 min

solutions for t_1 and t_2 respectively, with $t_1 = 2t_2$, an improved solution σ is given by

$$3\bar{\sigma} = 4\sigma_2 - \sigma_1 , \tag{3.5}$$

and the error is estimated to be $O(t_2^3)$ (see Smith [5, p. 140]). The improved values, denoted by a bar $\overline{(\ )}$, can be obtained from solutions having $t_1 = 0.4$, $t_2 = 0.2$, $Z = 15$.

The Gauss-Seidel explicit method of iteration when applied to the system (3.1) is not stable for all combinations of t and Z. As seen from the numerical results, this is due to the behavior of ψ for large ζ and φ for large η; i.e., $\psi \sim \zeta$ as $\zeta \to \infty$. Due to the appearance of ψt, φt, ηt, and ζt terms in (3.1a) and (3.1b), increasing the asymptotic boundary Z for fixed t ultimately leads to an instability, originating at large η, ζ, in the iterative procedure. Solutions for fixed t are found only for Z less than some Z_t. The values of Z_t for selected values of t are given in Table 2. Therefore, it was not possible to obtain a $t = 0.4$, $Z = 15$ solution directly. Although the instability might be eliminated by an implicit iterative scheme of the Peaceman-Rachford alternating direction type (Smith [5]), this additional complexity was deemed unnecessary for the analysis presented here. In lieu of an implicit calculation, a solution is obtained for $t = 0.4$, $Z = 10$. In order to provide the $Z = 15$ accuracy for the boundary values applied at $Z = 10$, the results along $\zeta = 10$, for $0 \leq \eta < 10$, of the $t = 0.2$, $Z = 15$ solution are applied as the boundary values at $Z = 10$ in the $t = 0.4$ calculation, in place of the asymptotic values (2.8). Therefore, for $0 \leq \zeta < 10$ solutions having the accuracy associated with $t = 0.4$, $Z = 15$ and $t = 0.2$, $Z = 15$ are determined.

The improved solution discussed previously can now be specified for $0 \leq \zeta < 10$.

The constant χ is also determined iteratively. The initial solutions for $\chi = 0$ were unacceptable in view of the algebraic behavior of all the flow variables as $\zeta \to \infty$. Furthermore, the values of $C(\eta, \zeta)$ and $V(\eta, \zeta)$ were in excess of those compatible with an error due solely to the finite difference approximation. $C(\eta, \zeta)$ was positive throughout with almost a uniform distribution; for $t = 0.2$, $Z = 10$, it was found that max $|C(\eta, \zeta)$, $V(\eta, \zeta)| = 0.08$. Near the corner where the streamwise velocity and vorticity are small,

TABLE 2

t	0.8	0.6	0.4	0.2
Z_t	<9	≈9	≈11	≈18

the errors in these quantities were therefore quite large. With algebraic decay, errors of $O(Z^{-1})$ in the outer boundary conditions are incurred and the dilemma is resolved. Due to the inaccuracy in the asymptotic formulas (2.8), when $\chi = 0$, additional mass crosses the outer boundary and is reflected as interior mass sources, compatible with Eqs. (2.9). These mass sources should decrease in strength as conditions (2.8) are more closely satisfied. That this is the case is shown in Fig. 3. For increasing positive χ the strength of the interior source points monotonically increases, while for increasing negative values of χ they are diminished until a minimum is attained. In Fig. 3, the maximum absolute value of $C(\eta, \zeta)$ is depicted as a function of χ for various t and Z. The increased accuracy with finer grid spacing t or larger values of Z is also shown. Similar variations with Z and t occur for $V(\eta, \zeta)$, although the maximum value for all of the solutions is almost insensitive to changes in χ, and for the improved solution, extremely small. Due to the zero boundary conditions for V on the surface and along the symmetry line, and the small value of V_ζ (or $\varphi_{\zeta\zeta}$) at $\zeta = Z$, the magnitude of $V(\eta, \zeta)$ is primarily a function of the grid spacing t, and only for the smaller value of $t = 0.2$ is the effect of the outer boundary significant. For the improved solution the error associated with the grid size is minimal and variations in χ have a minor influence. The same is not true for $C(\eta, \zeta)$ where derivative conditions apply at the surface and symmetry line. The asymptotic value of C (or ψ_ζ) at $\zeta = Z$ will be considerably larger and therefore variations in χ and Z have significant effects on $C(\eta, \zeta)$ for all of the t values shown on Fig. 3.
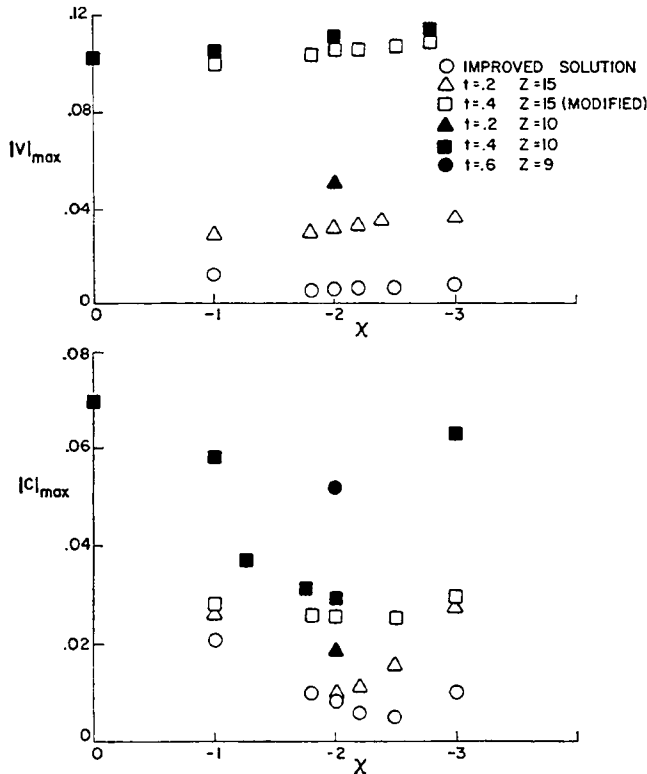

FIG. 3. Variation of $|c|$ and $|v|$ with χ, t and Z.

TABLE 3a. $C(\eta, \zeta)$

η	.8	1.6	2.4	3.2	4.0	4.8	5.6	6.4	7.2	8.0	8.8
8.8											.004
8.0										.004	.004
7.2									.003	.003	.004
6.4								.002	.002	.003	.003
5.6							.001	.001	.002	.003	.003
4.8						−.000	.000	.001	.001	.002	.003
4.0					−.001	−.000	−.000	.000	.001	.001	.002
3.2				−.002	−.001	−.001	−.000	−.000	.000	.001	.001
2.4			−.002	−.002	−.001	−.001	−.001	−.000	−.000	.000	.001
1.6		−.002	−.002	−.002	−.001	−.001	−.001	−.001	−.000	−.000	.001
.8	−.002	−.002	−.001	−.001	−.001	−.001	−.001	−.001	−.001	−.001	−.001
0.0	−.004	−.002	−.000	.001	.001	−.001	−.001	−.001	−.002	−.002	−.002
ζ	.8	1.6	2.4	3.2	4.0	4.8	5.6	6.4	7.2	8.0	8.8

It is noteworthy that for the improved solution the smallest maximum absolute value of $C(\eta, \zeta)$ occurs when $\chi = -2.5$, and corresponds to both the maximum negative and maximum positive values. For $\chi > -2.5$, Fig. 3 reflects a maximum negative value of $C(\eta, \zeta)$, with a positive maximum for $\chi < -2.5$. Furthermore, an average value of $C(\eta, \zeta)$ defined as the sum of all the interior values passes through zero at $\chi = -2.5$. Throughout the range $-2.7 < \chi < -2.3$ the effects of variations in χ are of the order of the series truncation error and therefore χ cannot be determined with any more precision. However, variations in the flow properties are minimal throughout this interval and $C(\eta, \zeta)$, $V(\eta, \zeta)$ remain quite small. Complete distributions of $C(\eta, \zeta)$ and $V(\eta, \zeta)$ are presented in Table 3 for $\chi = -2.5$. The results to be discussed in the following section relate to this solution.

4. Numerical results. In Table 4, the distributions of streamwise velocity and vorticity as well as the secondary flow velocities are presented. These solutions are in

TABLE 3b. $V(\eta, \zeta)$

η	.8	1.6	2.4	3.2	4.0	4.8	5.6	6.4	7.2	8.0	8.8
8.8											.000
8.0										.000	−.001
7.2									.000	−.001	−.001
6.4								.000	−.001	−.001	−.002
5.6							.000	−.001	−.001	−.001	−.002
4.8						.000	−.001	−.002	−.002	−.002	−.002
4.0					.000	−.002	−.003	−.003	−.003	−.003	−.002
3.2				.000	.000	−.002	−.003	−.003	−.003	−.003	−.002
2.4			.000	.000	−.000	−.002	−.003	−.003	−.004	−.004	−.004
1.6		.000	−.001	−.002	−.004	−.005	−.006	−.006	−.006	−.005	−.004
.8	.000	−.000	−.001	−.003	−.005	−.007	−.007	−.007	−.007	−.005	−.003
0.0	.000	.000	.000	.000	.000	.000	.000	.000	.000	.000	.000
ζ	.8	1.6	2.4	3.2	4.0	4.8	5.6	6.4	7.2	8.0	8.8

TABLE 4a. *Streamwise velocity u*

η	.8	1.6	2.4	3.2	4.0	4.8	5.6	6.4	7.2	8.0	8.8
8.8											1.000
8.0										1.000	1.000
7.2									1.000	1.000	1.000
6.4								1.000	1.000	1.000	1.000
5.6							1.000	1.000	1.000	1.000	1.000
4.8						.998	.999	1.000	1.000	1.000	1.000
4.0					.966	.989	.994	.996	.996	.997	.997
3.2				.815	.905	.950	.966	.971	.974	.975	.976
2.4			.543	.677	.781	.842	.869	.880	.885	.888	.890
1.6		.263	.381	.487	.573	.629	.657	.670	.677	.680	.682
.8	.068	.134	.195	.251	.297	.329	.346	.355	.359	.361	.362
0.0	.000	.000	.000	.000	.000	.000	.000	.000	.000	.000	.000

ζ

TABLE 4b. *Streamwise vorticity Ω*

η	.8	1.6	2.4	3.2	4.0	4.8	5.6	6.4	7.2	8.0	8.8
8.8											−.000
8.0										−.000	−.000
7.2									.000	−.000	−.000
6.4								.000	−.000	−.000	−.000
5.6							.000	−.002	−.002	−.002	−.001
4.8						.000	−.043	−.035	−.028	−.024	−.022
4.0					−.000	−.332	−.308	−.250	−.216	−.196	−.184
3.2				.000	−.898	−1.158	−1.035	−.905	−.830	−.785	−.756
2.4			−.000	−.783	−1.560	−1.813	−1.731	−1.617	−1.539	−1.488	−1.453
1.6		.000	−.252	−.721	−1.160	−1.338	−1.325	−1.264	−1.207	−1.159	−1.122
.8	−.000	−.049	−.113	−.171	−.193	−.161	−.095	−.027	.031	.082	.128
0.0	−.023	−.068	.027	.293	.601	.837	.985	1.075	1.131	1.169	1.202

ζ

TABLE 4c. *Secondary velocity v*

η	.8	1.6	2.4	3.2	4.0	4.8	5.6	6.4	7.2	8.0	8.8
8.8											1.779
8.0										1.839	1.773
7.2									1.919	1.831	1.758
6.4								2.029	1.909	1.810	1.731
5.6							2.190	2.014	1.877	1.772	1.690
4.8						2.422	2.160	1.958	1.814	1.709	1.631
4.0					2.580	2.334	2.043	1.840	1.705	1.612	1.545
3.2				2.111	2.293	2.054	1.788	1.615	1.508	1.437	1.388
2.4			1.079	1.615	1.727	1.545	1.346	1.220	1.146	1.100	1.070
1.6		.297	.643	.914	.963	.861	.746	.672	.629	.604	.590
.8	.026	.094	.195	.270	.280	.247	.210	.186	.172	.164	.160
0.0	0.000	0.000	0.000	0.000	0.000	0.000	0.000	0.000	0.000	0.000	0.000

ζ

TABLE 4d. *Secondary velocity w*

η	.8	1.6	2.4	3.2	4.0	4.8	5.6	6.4	7.2	8.0	8.8
8.8											1.779
8.0										1.839	1.838
7.2									1.919	1.915	1.904
6.4								2.029	2.021	2.001	1.974
5.6							2.190	2.173	2.136	2.092	2.047
4.8						2.422	2.396	2.328	2.252	2.179	2.113
4.0					2.580	2.621	2.531	2.410	2.298	2.200	2.118
3.2				2.111	2.349	2.370	2.271	2.145	2.028	1.928	1.843
2.4			1.079	1.326	1.413	1.400	1.327	1.232	1.141	1.059	.990
1.6		.297	.433	.418	.327	.231	.144	.065	−.005	−.065	−.117
.8	.026	.076	.061	−.048	−.188	−.305	−.388	−.447	−.491	−.525	−.554
0.0	0.000	0.000	0.000	0.000	0.000	0.000	0.000	0.000	0.000	0.000	0.000

The bottom row of the table is labelled ζ.

accord with the asymptotic behavior predicted in [2]. The streamwise velocity and vorticity exhibit a very rapid decay into the potential flow as η, $\zeta \to \infty$, but the algebraic nature of the flow for $\zeta \to \infty$, $\eta/\zeta \to 0$ is also apparent. As predicted by the asymptotic theory, the velocities u and v approach their boundary layer values somewhat more rapidly than does the crossflow velocity w or streamwise vorticity Ω. Moreover, for $\eta = \zeta \geq 4$, where series (2.8) is expected to deviate from the exact asymptotic solution by less than 10%, the computed numerical solutions are within 6% of the asymptotic formulas (2.8). For small values of η the accuracy of the asymptotic series is only good for much larger ζ, but deviations from the numerical solutions are always less than the series truncation error (see Appendix I).

Fig. 4 depicts isovels of the streamwise velocity. Included in the figure are the results found by Carrier [6] and Pearson [3], both of whom were unaware of the algebraic nature of the asymptotic flow field. Carrier obtained approximate solutions for u by splitting the continuity equation (2.1c) and neglecting the vorticity equation (2.1b). This procedure results in an erroneous secondary flow field, as shown by Rubin [1]. The results obtained here for mainstream velocity in the corner layer also differ significantly from those found by the Carrier approximation. The solutions found by Pearson [3], who solved the full set of corner layer equations by an iterative technique, are much better for the secondary[2] and streamwise velocities, although the secondary flows are significantly different for larger values of ζ (Fig. 5). This is to be expected in view of the algebraic decay. The corner layer thickness, defined here to be at the point where the shear stress $(u_\eta)_0$ is 99% of the two-dimensional value (Fig. 6), is about three to four two-dimensional flat plate boundary layer thicknesses.

The skin friction coefficient at $\eta = 0$ is defined by $(2\nu/U_0 x)^{1/2}(u_\eta)_0$. As shown in Fig. 6, this coefficient increases monotonically from zero at the corner to its asymptotic two-dimensional value. There are no overshoots in the skin friction similar to those found for the cold wall hypersonic interaction in a corner (Cresci et al. [7]), where the theory, applied only near the leading edge of the corner, fails to indicate a crosswise

---

[2] The secondary flow velocities for $\eta = \zeta \leq 3$ are relatively insensitive to variations in χ, but with $\chi = -2.5$ they are in excellent agreement with the asymptotic series (2.8).
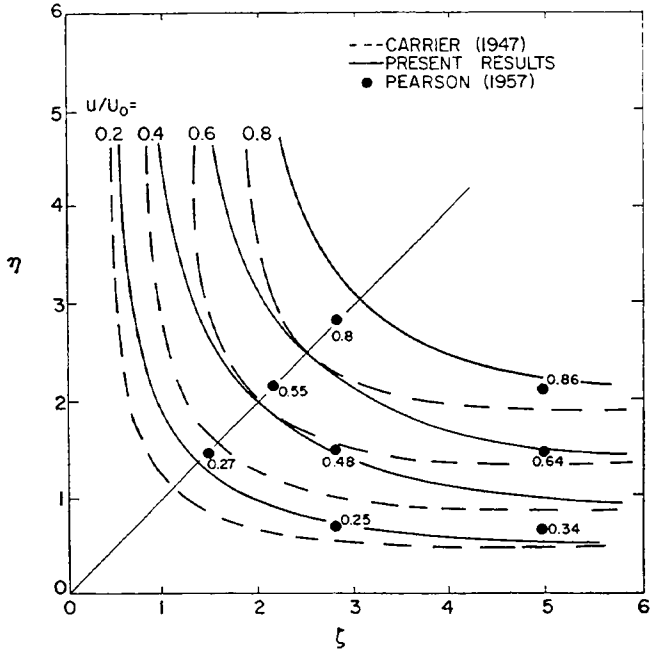
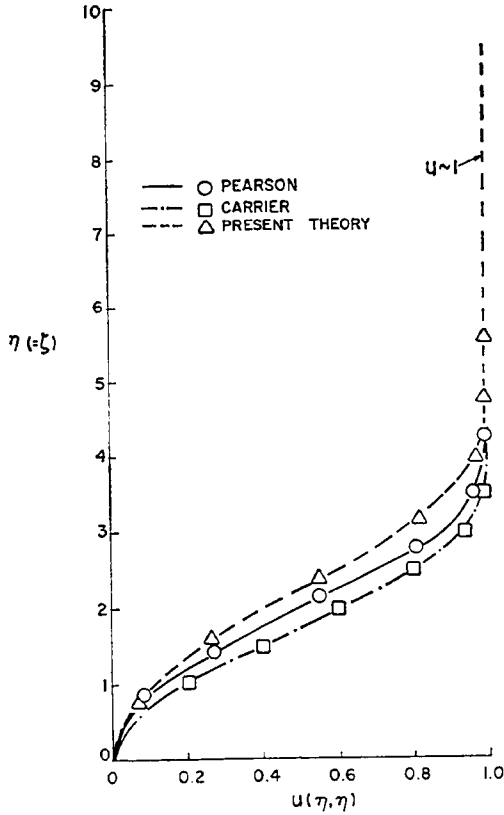FIG. 4.   Streamwise isovels.

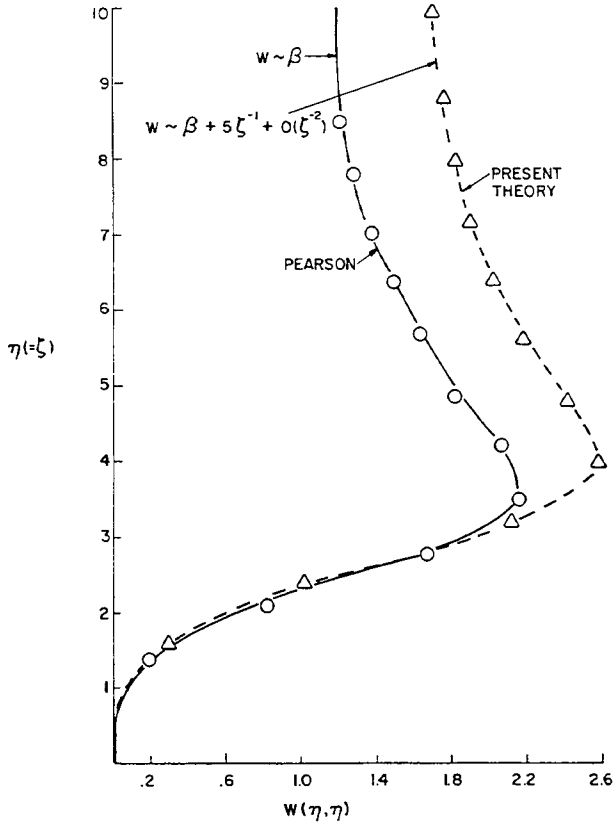FIG. 5a.   Streamwise velocity along symmetry line.

FIG. 5b.   Secondary velocities along symmetry line.
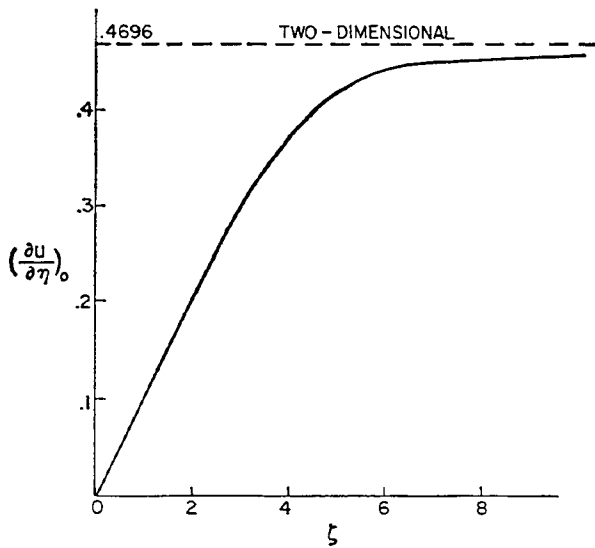

FIG. 6.   Skin friction in corner layer.

influx. On the other hand, Bloom [8] and Libby [9] independently have shown that the asymptotic inflow is eliminated for cold wall conditions even at very low Mach numbers. This would indicate a basic difference in the corner flow structure for cold wall and adiabatic wall conditions. Of course, the hypersonic corner layer interaction itself may be fundamentally different from the low-speed flow as the appearance of complex shock patterns will affect the structure of the secondary flow.

The computed secondary flow field is also described in Table 5, where the local crossflow direction as defined by $\tan^{-1}(w/v)$ is given. The region of inflow diminishes as ζ increases but a closed vortical flow in the corner layer is not established. In view of the asymptotic form of $w = R^{-1/2}w(\eta, z/x)$ in the boundary layer as $z/x \to \infty$, $[w(\eta, z/x) \sim 0.861f'(\eta)(z/x)^{-1/2}]$ (Rubin [1]), Fig. 7 represents a qualitative sketch of the entire boundary layer-corner layer secondary flow field. The crossflow velocity is locally tangent to the projected stream surfaces. The known corner layer and asymptotic boundary layer flow $(z/x \to \infty)$ are given by the solid and dashed lines, respectively. The intermediate region has not been determined but since the v velocity component is "Blasius" throughout to $O(R^{-1/2})$, the dotted lines are indicative of the flow in this region.

5. Summary. The flow along a corner formed by the intersection of two perpendicular flat plates leads to a three-dimensional boundary layer problem for the interior corner layer region. The governing equations are reduced to four Poisson-like equations and solved numerically by the Gauss-Seidel method of successive iteration. Since Pal and Rubin [2] have previously demonstrated the algebraic nature of the asymptotic flow field as $\zeta \to \infty$, terms up to $O(\zeta^{-2})$ in the series found in [2] are used as the asymptotic boundary values for the numerical analysis. A single arbitrary constant in this series is unknown. By varying the numerical value of this constant the mass flux across the outer boundary is altered and interior mass sources appear. The correct value of the constant is then determined by eliminating the appearance of such source effects. The final result should be accurate to within approximately two percent and is obtained by a suitable combination of solutions that have grid spacings of $t = 0.4$ and $t = 0.2$, respectively. The numerical results differ from the asymptotic series of [2] by less than

TABLE 5. *Secondary flow direction*

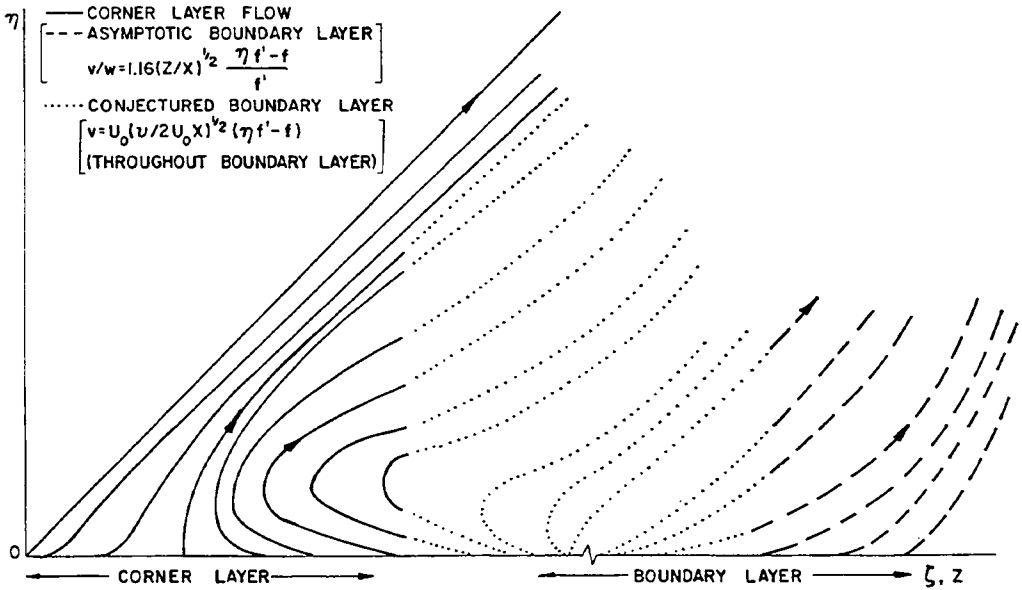| η		90°									
8.8											45
8.0										45	43
7.2									45	43	42
6.4								45	43	42	41
5.6							45	42	41	40	39
4.8		180°←		→0°		45	42	40	38	38	37
4.0					45	41	38	37	36	36	36
3.2				45	44	40	38	36	36	36	36
2.4			45	50	50	47	45	44	45	46	47
1.6		45	56	65	71	74	79	84	179	173	168
.8	45	51	72	170	146	129	118	112	109	107	106
	.8	1.6	2.4	3.2	4.0	4.8	5.6	6.4	7.2	8.0	8.8	ζ

FIG. 7.   Qualitative sketch of secondary flow (lines denote streamsurface intersection with crossplane).

6% in the range $\eta = \zeta \geq 4$ and deviations between the two values are always bounded by the series truncation error. In view of the algebraic decay, the corner layer extends outward approximately three to four two-dimensional flat plate boundary layer thicknesses. Although a swirling motion is found in the corner layer, a closed vortical pattern is not established for the incompressible flow.

Appendix I.   *Solution for $h(\eta)$ and $l(\eta)$.* The asymptotic series (2.7) can be written as

$$u \sim f'(\eta) + \chi \eta f''(\eta)\zeta^{-2} + \chi\beta(l'(\eta)/2 - h(\eta))\zeta^{-3} + O(\zeta^{-4}), \tag{I.1a}$$

$$\varphi \sim f(\eta) + \chi[3\eta f'(\eta) + f(\eta)]\zeta^{-2} + \chi\beta l(\eta)\zeta^{-3} + O(\zeta^{-4}), \tag{I.1b}$$

$$\psi \sim \zeta f'(\eta) - \beta g(\eta) + \chi[\eta f''(\eta) + 4f'(\eta)]\zeta^{-1} + \chi\beta h(\eta)\zeta^{-2} + O(\zeta^{-3}), \tag{I.1c}$$

$$\theta \sim \zeta f''(\eta) - \beta g'(\eta) + \chi f''(\eta)[5 - \eta f(\eta)]\zeta^{-1} + \chi\beta h'(\eta)\zeta^{-2} + O(\zeta^{-3}). \tag{I.1d}$$

The governing equations for the functions $h = h(\eta)$ and $l = l(\eta)$, as presented in [2], become

$$h''' + fh'' + 2f'h' + f''h = f'l'' - f'''l + g''(3\eta f' + f)$$
$$+ 2\eta f''g' - gf''(5 - \eta f), \tag{I.2a}$$

and

$$l''' + fl'' - 3f'l + 2f''l = 2(h'' + fh' - 3f'h) - 4\eta f''g. \tag{I.2b}$$

The boundary conditions are

$$h(0) = l(0) = l'(0) = 0,$$
$$h'(\eta) \sim o(\eta^{-N}), \qquad l'(\eta) - 2h(\eta) \sim o(\eta^{-M}) \quad \text{as} \quad \eta \to \infty \tag{I.3a}$$

for arbitrary M, N. The remaining boundary condition is obtained from symmetry (cf. P-R). Using the expansion (2.6), it is found that

$$h(\eta) \sim 1 + o(\eta^{-N}) \quad \text{as } \eta \to \infty \text{ for arbitrary } N. \tag{I.3b}$$

Eq. (I.2a) can be integrated once, and with (I.3b) becomes

$$h'' + fh' + f'h = f'l' - f''l - g(\eta f'' + 4f') + g'(3\eta f' + f) + 3. \tag{I.4}$$

The system (I.2b), (I.4) can be further simplified by introducing

$$s = s(\eta) = l' - 4h, \qquad t = t(\eta) = l. \tag{I.5}$$

Then

$$s'' + fs' - f's = 2g(4f' - \eta f'') - 2g'(3\eta f' + f) - 6, \tag{I.6a}$$

and

$$t''' + ft'' - 3f't' + 4f''t = 2f's - 2g(4f' + \eta f'') + 2g'(3\eta f' + f) + 6. \tag{I.6b}$$

The boundary conditions (I.3) transform as

$$s(o) = 0, \qquad t(o) = 0, \qquad t'(o) = 0, \qquad t' \sim 2 + o(\eta^{-N}),$$
$$s \sim -2 + o(\eta^{-M}), \tag{I.7}$$

as $\eta \to \infty$, for arbitrary N, M. $s(\eta)$ is first determined from (I.6a), with $t(\eta)$ obtained from (I.6b). The system is linear so that the two-point boundary value problem is solved by the suitable addition of complementary and particular solutions. The homogeneous equations exhibit both algebraically growing ($s \sim \eta$, $t' \sim \eta^3$) and exponentially decaying solutions. The algebraic growth is eliminated when the complimentary and particular solutions are combined. The functions $h(\eta)$ and $l(\eta)$ are presented in Table I.1.

Having determined the solution for the series (I.1), it is possible to examine the magnitudes of the specific terms and exhibit the divergent nature of the expansion. At $\eta = 2.0$, with $\chi = -2.5$, the largest overall errors are incurred by the truncated series (I.1). For $\zeta \gg 2$,

$$u \sim 0.817 - 1.28\zeta^{-2} + 4.96\zeta^{-3} + O(\zeta^{-4}),$$
$$\varphi \sim 0.887 - 14.47\zeta^{-2} + 71.62\zeta^{-3} + O(\zeta^{-4}),$$
$$\psi \sim 0.817\zeta + 0.187 - 9.45\zeta^{-1} + 18.26\zeta^{-2} + O(\zeta^{-3}),$$
$$\theta \sim 0.256\zeta - 1.12 - 2.87\zeta^{-1} - 6.68\zeta^{-2} + O(\zeta^{-3}), \tag{I.8}$$
$$v \sim 0.747 + 11.91\zeta^{-2} - 61.70\zeta^{-3} + O(\zeta^{-4}),$$
$$w \sim -0.187 + 8.17\zeta^{-1} - 13.30\zeta^{-2} + O(\zeta^{-3}),$$

Along $\eta = \zeta \gg 1$, from (2.8),

$$u \sim 1 + o(\zeta^{-M}), \qquad \theta \sim o(\zeta^{-N}), \quad M, N \quad \text{arbitrary positive}, \tag{I.9}$$
$$v = w \sim 1.2168 + 5\zeta^{-1} + 1.522\zeta^{-2} + O(\zeta^{-3}).$$

Therefore, with $\zeta = Z = 15$, the error near the boundary associated with the truncated series (2.8) should be less than 0.02 for any of the physical flow properties. The series (I.9) is in excellent agreement with the numerical solution for $\zeta \geq 3.5$; e.g., at $\zeta = 4$

TABLE I.1. $h(\eta)$, $l(\eta)$

η	$h(\eta)$	$h'(\eta)$	$l(\eta)$	$l'(\eta)$
0.0	0.0000	-6.9426	0.0000	0.0000
.4	-2.5336	-5.7080	-1.3400	-6.5287
.8	-4.5386	-4.2651	-5.0631	-11.8467
1.2	-5.8923	-2.4264	-10.5845	-15.4150
1.6	-6.4205	$-.1569$	-17.0804	-16.6358
2.0	-6.0048	2.1948	-23.5452	-15.2742
2.4	-4.7515	3.8985	-29.0191	-11.8329
2.8	-3.0566	4.3487	-32.8917	-7.4986
3.2	-1.4333	3.6156	-35.0713	-3.5521
3.6	$-.2341$	2.3565	-35.8895	$-.7529$
4.0	.4721	1.2334	-35.8357	.8447
4.4	.8096	.5260	-35.3275	1.5899
4.8	.9421	.1846	-34.6242	1.8769
5.2	.9851	.0537	-33.8514	1.9687
5.6	.9968	.0130	-33.0578	1.9933
6.0	.9994	.0026	-32.2591	1.9988
6.4	.9999	.0004	-31.4594	1.9998
6.8	1.0000	.0001	-30.6594	2.0000
7.2	1.0000	.0000	-29.8594	2.0000
7.6	1.0000	.0000	-29.0594	2.0000
8.0	1.0000	.0000	-28.2594	2.0000
8.4	1.0000	$-.0000$	-27.4594	2.0000
8.8	1.0000	$-.0000$	-26.6594	2.0000
9.2	1.0000	$-.0000$	-25.8594	2.0000
9.6	1.0000	$-.0000$	-25.0594	2.0000

and $\zeta = 5.6$, the numerical results are $w = 2.580$ and $w = 2.190$, respectively, while from (I.9) we obtain $w = 2.512$ and $w = 2.158$.

Appendix II. Finite difference approximation. For a function $T_0 = T(\eta, \zeta)$ having continuous third-order partial derivatives in η, ζ, Taylor's series expansion gives

$$T_1 = T(\eta + t, \zeta) = T_0 + tT_{0_\eta} + (t^2/2)T_{0_{\eta\eta}} + (t^3/6)T_{0_{\eta\eta\eta}} + O(t^4), \qquad \text{(II.1a)}$$

and

$$T_3 = T(\eta - t, \zeta) = T_0 - tT_{0_\eta} + (t^2/2)T_{0_{\eta\eta}} - (t^3/6)T_{0_{\eta\eta\eta}} + O(t^4) \qquad \text{(II.1b)}$$

with similar relations for $T_2 = T(\eta, \zeta + t)$, $T_4 = T(\eta, \zeta - t)$.

Therefore, the following derivative relations are obtained:

$$t^2 T_{0_{\eta\eta}} = T_1 + T_2 - 2T_0 + O(t^4), \qquad \text{(II.2a)}$$

and

$$2t T_{0_\eta} = T_1 - T_3 + O(t^3), \qquad \text{(II.2b)}$$

with similar results for $T_{0_{\zeta\zeta}}$, T_{0_ζ}. If the relations (II.1), (II.2) are used in the governing equations, the finite difference system (3.1) results.

The truncation error denoted by $\|(\ )\|$ and defined as the difference between Eqs. (3.1) and the governing system of partial differential equations (2.2) and (2.4) is given by

$$||(3.1\text{a})|| = (t^2/12)\{u_{0_{\eta\eta\eta\eta}} + u_{0_{\zeta\zeta\zeta\zeta}} + 2\varphi_0 u_{0_{\eta\eta\eta}} + 2\psi_0 u_{0_{\zeta\zeta\zeta}}\}, \tag{II.3a}$$

$$||(3.1\text{b})|| = (t^2/12)\{\theta_{0_{\eta\eta\eta\eta}} + \theta_{0_{\zeta\zeta\zeta\zeta}} + 2\varphi_0\theta_{0_{\eta\eta\eta}} + 2\psi_0\theta_{0_{\zeta\zeta\zeta}} + 4\zeta u_0 u_{0_{\eta\eta\eta}} - 4\eta u_0 u_{0_{\zeta\zeta\zeta}}\},$$

$$\tag{II.3b}$$

$$||(3.1\text{c})|| = (t^2/12)\{\varphi_{0_{\eta\eta\eta\eta}} + \varphi_{0_{\zeta\zeta\zeta\zeta}} + 2\theta_{0_{\zeta\zeta\zeta}} - 4u_{0_{\eta\eta\eta}}\}, \tag{II.3c}$$

$$||(3.1\text{d})|| = (t^2/12)\{\psi_{0_{\eta\eta\eta\eta}} + \psi_{0_{\zeta\zeta\zeta\zeta}} - 2\theta_{0_{\eta\eta\eta}} - 4u_{0_{\zeta\zeta\zeta}}\}. \tag{II.3d}$$

Therefore the truncation errors (II.3) and discretization errors (II.1) are $O(t^2)$. The maximum errors in (II.3) are a result of the asymptotic form of ψ_0 and θ_0, which asymptote to $\zeta f'(\eta) - \beta g(\eta)$ and $\zeta f''(\eta) - \beta g'(\eta)$ respectively. Higher-order derivatives of these expressions are maximal in the vicinity of $\eta = 1.5$ where errors in $V(\eta, \zeta)$ are largest. These inaccuracies are substantially reduced for the improved solution where the truncation error is $O(t^3)$.

References

[1] S. G. Rubin, *Incompressible flow along a corner*, J. Fluid Mech. 26, part 1, 97–110 (1966)

[2] A. Pal and S. G. Rubin, *Asymptotic features of the viscous flow along a corner*, Quart. Appl. Math. 29, 91 (1971)

[3] J. R. A. Pearson, *Homogeneous turbulence and laminar viscous flow*, Ph.D. Thesis, Cambridge University, 1957

[4] L. Rosenhead, editor, *Laminar boundary layers*, Clarendon Press, Oxford, 1963

[5] G. D. Smith, *Numerical solution of partial differential equations*, Oxford University Press, London, 1965

[6] G. Carrier, *The boundary layer in a corner*, Quart. Appl. Math. 4, 367–370 (1947)

[7] R. J. Cresci, S. G. Rubin, C. T. Nardo and T. C. Lin, *Hypersonic interaction along a rectangular corner*, AIAA J. 7, 2241–2246 (1969)

[8] M. H. Bloom, *Remark on compressibility effects in the boundary layer cross flow near a corner*, Polytechnic Institute of Brooklyn, PIBAL Report No. 969, 1966

[9] P. Libby, *Secondary flows associated with a supersonic corner region*, AIAA J. 4, 1130–1131 (1966)